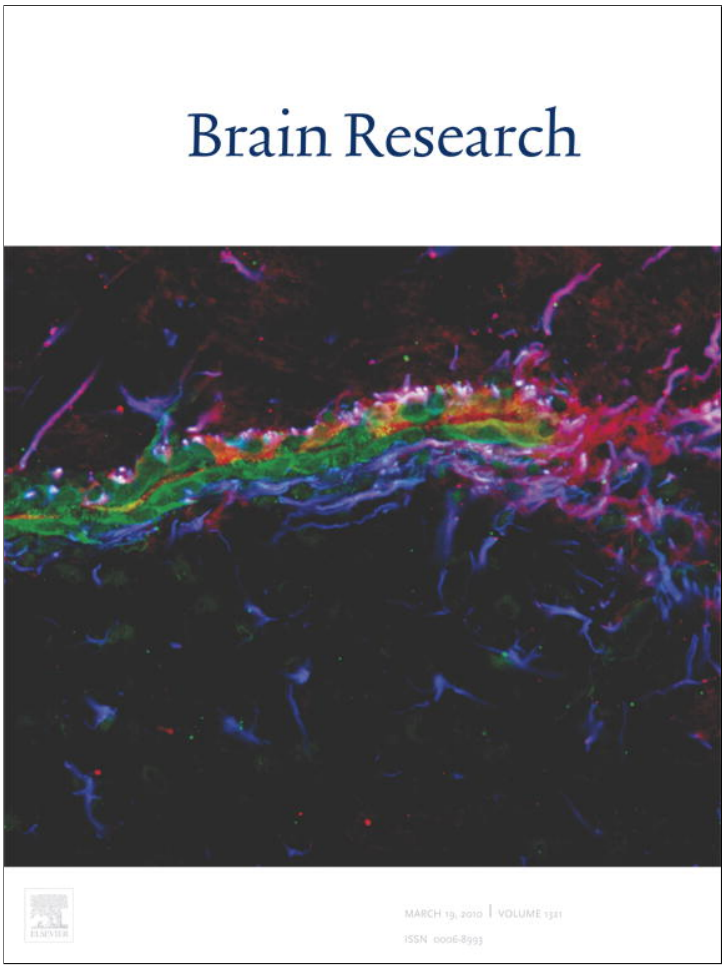

BRAIN RESEARCH 1321 (2010) 20–30

available at www.sciencedirect.com

www.elsevier.com/locate/brainres

BRAIN RESEARCH

Research Report

# Endothelinergic cells in the subependymal region of mice

*Mauricio M. Castañeda, Marisa A. Cubilla, Martín M. López-Vicchi, Angela M. Suburo**

*Facultad de Ciencias Biomédicas, Universidad Austral, Pilar, Buenos Aires B1629AHJ, Argentina*

ARTICLE INFO

*Article history:*
Accepted 20 January 2010
Available online 29 January 2010

*Keywords:*
Endothelin
Astrocyte
Subventricular zone
Subependymal zone
Cingulum
Adult neurogenesis
Granulocyte-colony stimulating factor
Neural stem cell
Stroke
Traumatic brain injury

ABSTRACT

Endothelin (ET) is a small peptide that activates astrocyte proliferation, regulates proliferation and migration of embryonic neural precursor cells and stimulates glioblastoma growth. We found that in mouse brain, ET and its receptor B (ETRB) were highly expressed in the subependymal zone (SEZ), an adult neurogenic niche. Cells with ET immunoreactivity ($ET^+$ cells) selectively appeared along the lateral and dorsal walls of the lateral ventricle. They also appeared in the cingular region of the corpus callosum. Subependymal $ET^+$ cells also displayed prominin (PRO), glial fibrillary acidic protein (GFAP) and ETRB immunoreactivities. $ET^+$ processes traversed the ependymal epithelium and approached the ventricular lumen. Ependymal cells only showed ETRB-ir. A small but consistent number of $ET^+$ cells displayed proliferation markers: 5-bromo-2′-deoxyuridine (BrdU) incorporation, and minichromosome maintenance protein 2 (Mcm2). Cortical injury and G-CSF increased subependymal endothelinergic cells and their proliferation markers. Our findings suggest that ET and ETRB might be associated with regulation of adult neural stem cells and their migration through neurogenic and gliogenic pathways.



## 1. Introduction

Endothelin (ET) is a 21-amino acid peptide originally identified in the conditioned medium of cultured endothelial cells (Davenport and Maguire, 2006). The ET family includes at least three peptides (ET-1, ET-2, and ET-3) and two receptors (ETRA and ETRB). ET is seldom detected in normal brain astrocytes (Ostrow and Sachs, 2005). However, several studies have shown ET in cultured (Ehrenreich et al., 1991) and reactive astrocytes (Gadea et al., 2008). These glial cells are targets for ET-1-induced activation, including cell proliferation (Rogers et al., 2003; Tabernero et al., 2006) and release of neurotrophic factors (Koyama et al., 2005). Both ET-1 and ETRB expression are strongly up-regulated in reactive astrocytes (Iribarne et al., 2008; Ostrow and Sachs, 2005; Torbidoni et al., 2005).

Endothelins also regulate proliferation and migration of embryonic neural precursor cells (Mizuno et al., 2005; Morishita et al., 2007; Shinohara et al., 2004). In addition, these peptides can stimulate growth of brain malignant tumors, such as glioblastoma (Paolillo et al., 2006) and astrocytoma (Naidoo et al., 2005).

Neural stem cells (NSCs, also called neural progenitors) have been identified in germinal regions within the adult

* *Corresponding author*. Fax: +54 2322 48 2205.
E-mail addresses: amsuburo@cas.austral.edu.ar, amsuburo@gmail.com (A.M. Suburo).

*Abbreviations:* BrdU, 5-bromo-2′-deoxyuridine; CC, corpus callosum; CONTRA, contralateral; DVW, dorsal ventricular wall; EE, ependymal epithelium; ET, endothelin; ET-1, endothelin-1; ET-2, endothelin-2; ET-3, endothelin-3; ETRA, endothelin receptor A; ETRB, endothelin receptor B; G-CSF, Granulocyte-colony stimulating factor; GFAP, glial fibrillary acidic protein; IPSI, ipsilateral; LV, lateral ventricle; LVW, lateral ventricular wall; Mcm2, minichromosome maintenance protein-2; NES, nestin; PRO, CD133 prominin-1; RMS, rostral migratory stream; ROI, region of interest; SCE, subcallosal enlargement; SEZ, subependymal zone; SGZ, subgranular zone

0006-8993/$ – see front matter © 2010 Elsevier B.V. All rights reserved.
doi:10.1016/j.brainres.2010.01.056

mammalian brain: the subventricular or subependymal zone (SEZ) beneath the lateral ventricles, and the subgranular zone (SGZ) within the dentate gyrus of the hippocampus. In these regions, a special subpopulation of cells expressing glial fibrillary acidic protein (GFAP) originates transient amplifying progenitors and proliferating neuroblasts (Alonso et al., 2008; Doetsch et al., 1999; Garcia et al., 2004; Seri et al., 2001). However, the identity of true NSCs is still controversial (Duan et al., 2008). Evidence points out that activated CD133$^+$ ependymal cells might also serve as adult NSCs (Zhang et al., 2007). On the other hand, multipotential (neuronal–astroglial–oligodendroglial) precursors with stem cell features have been isolated not only from the SEZ but also from their derivatives along the rostral migratory stream (RMS) (Gritti et al., 2002; Platel et al., 2009).

In adult rat brains, intraventricular injection of an ETRB ligand increases the numbers of astrocytes, whereas an antagonist significantly decreases their numbers (Ishikawa et al., 1997; Koyama et al., 2003). Besides, the developing dentate gyrus of rats carrying a null mutation of *EDNRB* shows a raised rate of apoptosis (Riechers et al., 2004). Therefore, we studied immunohistochemical expression of ET and ETRB in cells of the SEZ neurogenic niche and neighboring regions, and their co-localization with known NSC markers. Next, we compared SEZ endothelinergic immunoreactivity under basal conditions and after cortical lesions. We also evaluated the effect of granulocyte-colony stimulating factor (G-CSF), a hematopoietic growth factor that controls proliferation and differentiation of neural stem cells (Diederich et al., 2009), on endothelinergic cells.

## 2. Results

### 2.1. *Localization of endothelinergic cells in normal mouse SEZ*

In the normal mouse brain, cells displaying ET immunoreactivity (ET$^+$ cells) consistently appeared along the walls of the lateral ventricle (LV). They had small cell bodies and showed bipolar or multipolar phenotypes. ET$^+$ cells gathered in the angle formed by lateral and dorsal ventricular walls (LVW and DVW). This subcallosal enlargement (SCE) was continuous with the rostral migratory stream (RMS) (Platel et al., 2009). A large cluster of ET$^+$ cells appeared around the ventral end of the ventricle, but we have not included them in this study. In addition, ET$^+$ cells were present in the corpus callosum (CC) (Fig. 1A). Marginal glia showed strong ET immunoreactivity, but cortical areas did not contain ET$^+$ cells.

Along the LVW, ET$^+$ cells and processes followed a distinct dorso-ventral pattern. Their number was highest in the dorsalmost segment of this wall, close to the SCE. Cells in this region often showed an elongated shape parallel to the ependymal wall (Fig. 1B). Fractones (Fig. 1C), often found on this ventricular wall, always contained ET$^+$ cells. The DVW also displayed many endothelinergic structures (Fig. 1D). Ependymal cells lacked ET immunoreactivity, but apical processes from ET$^+$ subependymal cells traversed the ependymal epithelium (EE) up to the VL lumen. Processes appeared across LVW and DVW (Figs. 1 and 2).

The SCE and RMS contained multipolar or bipolar ET$^+$ cells. Their processes formed a dense network resembling glial tube profiles (Lois et al., 1996; Peretto et al., 1997). In addition, ET$^+$ cells surrounded blood vessels.

Many multipolar ET$^+$ cells appeared in the CC, being most abundant in the cingulum bundle. Cingular ET$^+$ cells clustered close to the DVW, becoming sparser towards the apex of the cingulum.

This endothelinergic pattern appeared at all rostrocaudal levels examined, from +3 to −2 mm A–P from bregma (Paxinos and Franklin, 2001). Five anti-endothelin sera were tested (Table 1). The ET-1 specific antiserum produced the same immunoreactivity pattern as antisera recognizing ET-1 and ET-2, or the antiserum recognizing ET-1, ET-2 and ET-3. The anti-ET-3 specific serum produced little immunostaining.

In addition, immunostaining of consecutive coronal sections showed that ET$^+$ regions also exhibited strong GFAP-ir (Fig. 1E). Since these observations suggest a link between subependymal ET$^+$ cells and NSCs, we explored co-localization of ET with known neurogenic markers.

### 2.2. *Co-localization of ET-ir with NSC markers*

Nestin (NES), a class of intermediate filaments, is a widely used marker that distinguishes precursors from more differentiated cells in the neural tube (Abrous et al., 2005). In normal animals, NES was mainly expressed by EE cells and was not present in subependymal ET$^+$ cells. Thus, endothelinergic cell processes clearly contrasted among NES$^+$ epithelial cells (Fig. 2A). A few ET$^+$ structures also displayed NES-ir (not shown) within the SCE.

Prominin-1 (PRO, CD133) is a pentaspan membrane protein found in mouse neuroepithelial stem cells (Corti et al., 2007; Dubreuil et al., 2007). We observed complete co-localization of ET- and PRO-ir within the different regions of SEZ and CC (Figs. 2B–D). In addition, PRO-ir appeared in LVW and DVW ependymal cells.

Confocal microscopy proved that all ET$^+$ structures displayed GFAP-ir (Figs. 2C and D). The reverse was not true, since ET-ir was low or undetectable in GFAP$^+$ cells from other brain regions, such as striatal or septal astrocytes.

Cell processes traversing the EE displayed ET-ir with PRO- and GFAP-irs. Triple immunofluorescent processes appeared along the LVW and DVW. The latter were thicker than those from the LVW (Fig. 2C).

Cingular endothelinergic cells also presented PRO- and GFAP-irs (Fig. 2D), but NES$^+$ structures were not detected in the normal CC.

### 2.3. *Endothelinergic receptors*

Under basal conditions, ETRA was undetectable in the SEZ and neighboring callosal or striatal regions. ETRB, by contrast, appeared in subependymal endothelinergic cells and ependymal cells. The endothelium of small vessels beneath the ventricular lateral wall showed moderate ETRB-ir (Figs. 3A and B).

### 2.4. *Activation of endothelinergic subependymal cells by cortical lesions*

Focal cerebral ischemia activates neurogenesis in the SEZ and induces neuroblast migration towards the ischemic boundary (reviewed in Zhang et al., 2008). Therefore we evaluated ET-ir in the SEZ after devascularization of the motor cortex.

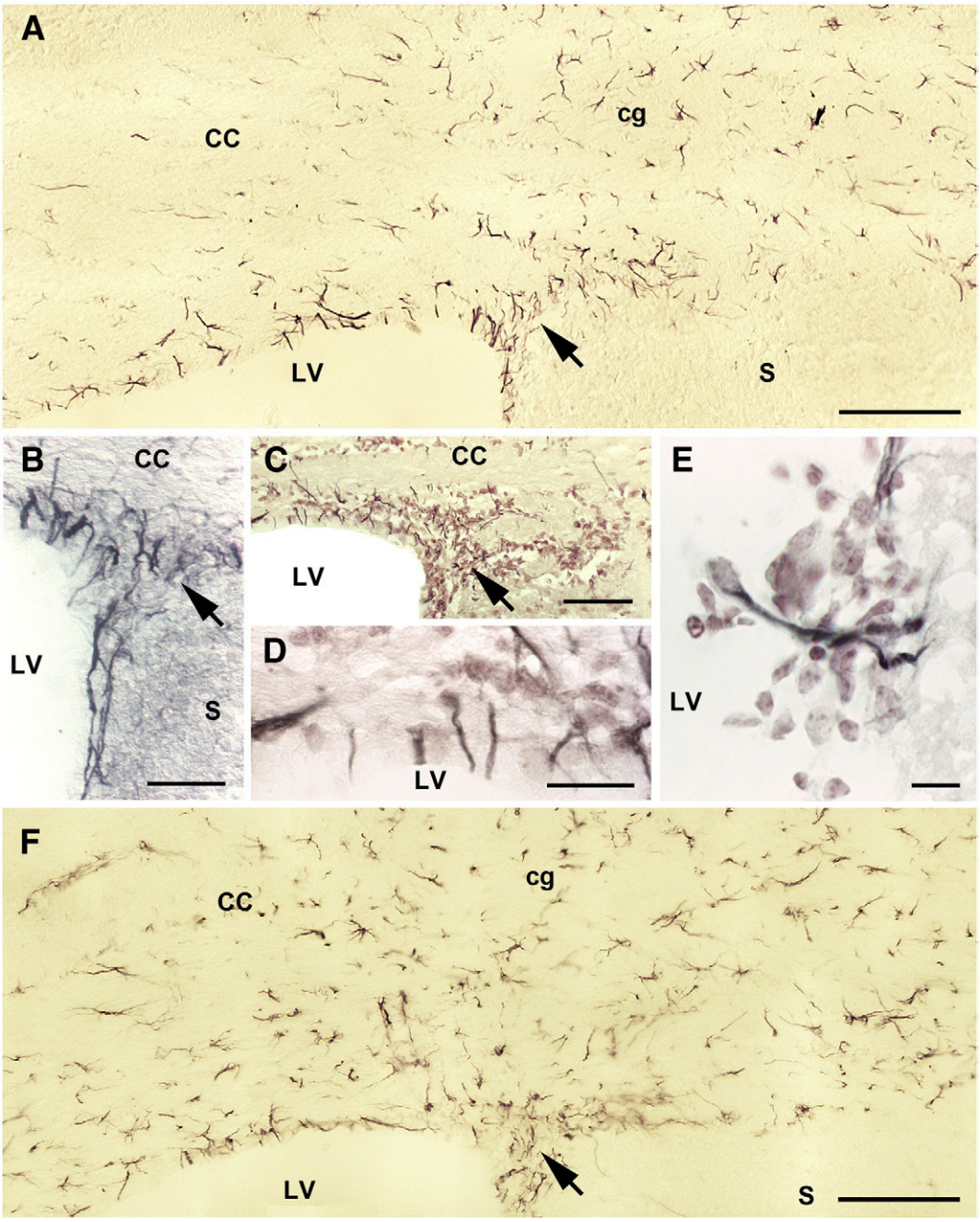


**Fig. 1 – Images in this plate show immunoenzymatic detection of ET (A–E) and GFAP (F) in SEZ and neighboring regions of control mice. Arrows point to the subcallosal enlargement (SCE). A. Endothelinergic structures appeared along LVW and DVW. Notice their clustering in SCE (arrow), in the angle between those ventricular walls. Callosal $ET^+$ cells selectively collected in the cingular region (cg). Bar, 100 μm. B. The dorsalmost part of the LVW and the SCE are shown at a larger magnification. Long and thick endothelinergic processes extend along the dorsalmost portion of the LVW. Processes also appear in the angle between lateral and dorsal walls. Bar, 25 μm. C. Counterstaining with Neutral Red shows that $ET^+$ structures form a network within a group of small and strongly stained nuclei lying along the LVW, the SCE and lateralmost part of the DVW. Bar, 50 μm. D. The DVW is shown at a larger magnification to illustrate the $ET^+$ cell processes traversing the ependymal epithelium. Bar, 25 μm. E. An endothelinergic cell is shown amidst a large collection of neutral red-stained nuclei forming a fractone. The $ET^+$ cell body appears close to the ventricular lumen and displays a long basal process. Bar 25 μm. F. GFAP immunostaining is shown in a coronal section, similar to that shown in A. GFAP-ir is more abundant than ET-ir. The difference is striking in the CC, where $GFAP^+$ structures do not cluster at the cingulum. Bar, 100 μm.**

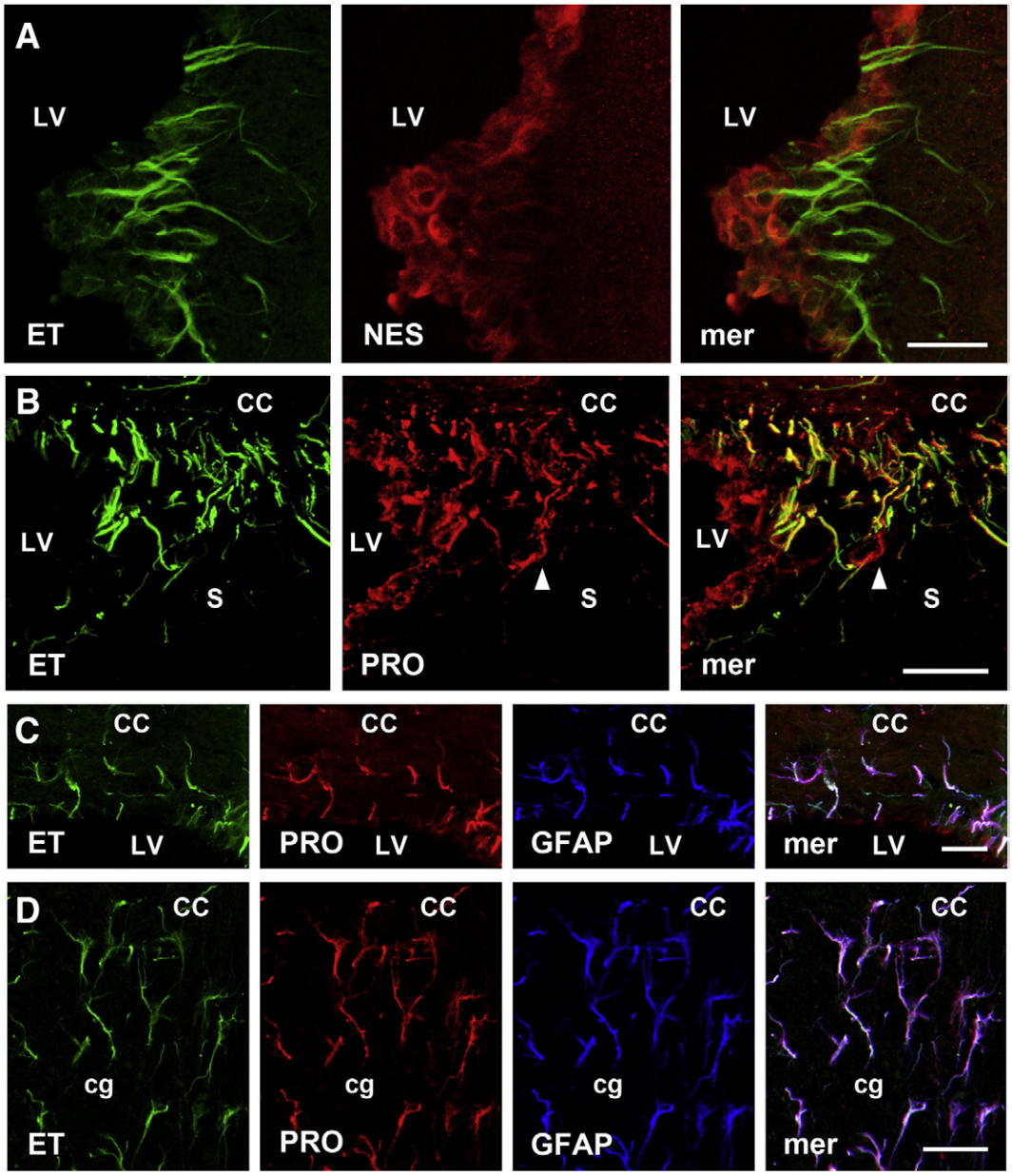


**Fig. 2 – Confocal imaging shows the SEZ of a normal animal. The four images correspond to a single optical slice (1 μm) simultaneously labeled for two or three of the following markers ET, NES, PRO or GFAP. Merges (mer) are shown at the right. A. ET$^+$ processes cross the ependymal layer of the LVW, as previously shown by the immunoenzymatic procedure. Ependymal cells showed NES-ir. The cluster of processes and ependymal cells belongs to a fractone. Bar, 25 μm. B. The SCE appears as a triangular region bounded by LVW, DVW, CC and S. It shows many ET$^+$ structures that are continuous with those found in the LVW and DVW. Most ET$^+$ structures also show PRO-ir. By contrast, PRO-ir is also observed in some non-endothelinergic processes (arrowheads) and in the ependymal epithelium. Calibration bar, 50 μm. C. A section of the DVW, close to the SCE (right side), shows co-localization of ET-, PRO- and GFAP-irs in cell processes traversing the ependymal epithelium. Bar, 25 μm. D. In the cingular region, cells show a similar immunostaining pattern. Bar, 25 μm.**

Five days after cortical devascularization, both ET- and ETRB-ir increased in the ipsilateral SEZ and cingulum. As in control animals, both immunoreactivities showed perfect co-localization in the SEZ and CC, whereas the EE displayed ETRB-ir but no ET-ir (Figs. 3A–D). Increases of GFAP-, PRO- and NES-irs accompanied the expansion of endothelinergic immunoreactivity. Subependymal cells displaying ET and its receptor B showed co-localization with GFAP- and PRO-ir (Figs. 3C and D).

### 2.5. *Endothelinergic cells and proliferation markers*

Many SEZ cells contained 5-bromo-2′-deoxyuridine (BrdU) after short incorporation periods. Most of them appeared along the

**Table 1 – Antibodies used in this study.**

| Antibody | Host | Source |
|---|---|---|
| ET-1 and Big-ET-1 | Rabbit PAB | Bachem, Torrance, CA (T-4572) |
| ET-1, ET-2 and Big-ET-1 | Guinea pig PAB | Bachem, Torrance, CA (T-5011) |
| ET-1, ET-2 and Big-ET-1 | Rabbit PAB | Bachem, Torrance, CA (T-4050) |
| ET-1, ET-2, ET-3 and Big-ET-1 | Rabbit PAB | Bachem, Torrance, CA (T-4495) |
| ET-3 | Rabbit PAB | Bachem, Torrance, CA (T-4317) |
| ETRA | Rabbit PAB | Alomone; Israel (AER-001) |
| ETRB | Rabbit PAB | Alomone, Israel (AER-002) |
| GFAP | Mouse MAB | Biogenex, San Ramon, CA (GA-5) |
| GFAP-Cy3 | Mouse MAB | Sigma-Aldrich Co, St Louis, MO (C9205) |
| Nestin | Goat PAB | Neuromics, Edina, MN (GT15114) |
| Nestin | Chicken MAB | Neuromics, Edina, MN (CH23001) |
| Prominin-1/CD-133 | Rat MAB | Millipore, Billerica, MA (MAB4310) |
| Mcm2 | Goat PAB | Santa Cruz Biotechnology, Santa Cruz, CA (sc9839) |
| BrdU | Mouse MAB | Stephen J. Kaufman, Developmental Studies Hybridoma Bank, Iowa City, Iowa (G3G4) |

LVW and within the SCE. Only the lateral part of the DVW, close to the SCE, showed some $BrdU^+$ cells.

Positive identification of $ET^+BrdU^+$ cells under confocal microscopy required recognition of perinuclear ET-ir in 5 or more consecutive optical sections. Their number was very low (Fig. 3E). In the LVW, only 3 $ET^+BrdU^+$ cells were scored in 32 sections from 6 different brains. $ET^+BrdU^+$ cells appeared more often in injured brains; 25 were scored in 22 sections from 6 different brains. Co-localization might be more extensive, since cytoplasmic ET-ir was much lower than ET-ir in cell processes. In addition, ET-ir partially degraded after the hydrolysis step used in BrdU detection.

We also made double stainings with Mcm2 (minichromosome maintenance protein-2), a protein involved in G1 permits for DNA replication, that is expressed by proliferative neuroprogenitors and by the slowly cycling NSCs of the brain (Maslov et al., 2004). $Mcm2^+$ nuclei appeared along the LVW, being most abundant within fractones. The SCE contained many $Mcm2^+$ nuclei, but only a few appeared along the DVW.

The LVW showed a few $ET^+Mcm2^+$ cells (4 cells in 32 sections from 9 different brains). $ET^+Mcm2^+$ cells were also present in SCE (Fig. 3F). As before, the strong immunostaining of endothelinergic cell processes hindered quantitative evaluation of perinuclear ET-ir. $GFAP^+Mcm2^+$ immunofluorescent cells appeared in the same localizations as $ET^+Mcm2^+$ cells. Most $Mcm2^+$ cells had neither ET- nor GFAP-irs.

$Mcm2^+$ nuclei increased after cortical devascularization, when they also expanded along the DVW. In the LVW we scored 12 cells in 10 sections from 6 brains. G-CSF treatment did not increase the density of $Mcm2^+$ cells (not shown) or the frequency of $ET^+Mcm2^+$ cells.

### 2.6. *Quantitative evaluation of endothelinergic immunoreactivity patterns*

We measured changes of $ET^+$ areas under two different experimental conditions: devascularization and G-CSF treatment. Since each SEZ region reacted differently to these neurogenic stimuli, we defined regions of interest (ROIs) for each zone.

#### 2.6.1. *Lateral ventricular wall*

ET-ir associated to the LVW included endothelinergic cells and processes along or within the ependymal lining. These were most abundant near the SCE than in more ventral regions (see Fig. 1). Therefore, we defined two ROIs, one for the dorsalmost 80 μm and another for the following 100 μm. More ventral portions usually displayed fractones. We reported ET-ir as immunoreactive area

**Fig. 3 – Confocal images in A, B, C and D compare ET and its receptor ETRB in the SEZ of control and devascularized mice. All images correspond to a single optical slice (1 μm) simultaneously labeled for ET, ETRB, PRO or GFAP. Merges (mer) are shown at the right. A. In a control mouse, the SCE displays $ET^+$ cells and processes. ETRB-ir appears in the same cells, but immunofluorescence is weak. ET-I, ETRB- and GFAP-ir colocalize in the same cellular structures (arrowheads). Ependymal cells display strong ETRB-ir, but do not show ET- or GFAP-ir. Bar, 50 μm. B. The LVW shows strong ETRB immunofluorescence in the ependymal lining, and in the endothelium of neighboring small blood vessels (arrowheads). $GFAP^+$ cells and processes are attached to the ventricular wall and to blood vessels. No co-localization is detected. Bar, 25 μm. C. The SCE region ipsilateral to a cortical devascularization has an abnormal morphology. Both the ependymal layer and neighboring SEZ cells show a high increase of ETRB immunofluorescence. PRO is also increased in ependymal cells and neighboring SEZ cells. $GFAP^+$ structures only appear in the SEZ. Arrowheads identify structures displaying the three markers, whereas short arrows point to structures showing only PRO and GFAP immunofluorescence. Bar, 50 μm. D. SEZ structures associated to the ipsilateral LVW of a devascularized animal show strong ET, ETRB and GFAP immunofluorescence. Most $ET^+$ and $GFAP^+$ structures lie beneath the ependymal wall, but thick cell processes extend into the striatum. ETRB has similar localizations but also appears in ependymal cells and cell nuclei. Bar, 25 μm. E. A 4 μm projection through the SCE illustrates an $ET^+$ cell (arrow), immediately beneath the EE (unstained), and an $ET^+BrdU^+$ cell (arrowhead). Bar (E to H), 10 μm. F. In a 5 μm projection, an $ET^+Mcm2^+$ cell (arrowhead) appears around a blood vessel close to the SCE. The vessel is surrounded by several $ET^+$ processes. G. This 1 μm optical section illustrates the LVW, ipsilateral to a cortical lesion. Many $Mcm2^+$ nuclei can be observed and arrowheads point to $ET^+Mcm2^+$ cells. H. An $ET^+Mcm2^+$ cell (arrowhead) appears in the callosal cingulum after an ipsilateral cortical lesion (5 μm projection).**

($\mu m^2$) by LVW length ($\mu m$). Average values of control specimens from devascularization and G-CSF experiments were similar.

Data from dorsalmost LVW samples passed D'Agostino–Pearson normality test and were compared using ANOVA followed by Tukey's test (Fig. 4A). The highest immunoreactivity levels appeared in the ipsilateral LVW of devascularized animals ($7.31 \pm 1.12\ \mu m^2$, $n=9$ sections, 3 brains). ET-ir in G-CSF samples ($2.75 \pm 0.31\ \mu m^2$, $n=22$ sections from 3 brains) were not significantly different from values detected in control brains ($1.97 \pm 0.29\ \mu m^2$, $n=22$ sections from 6 brains). In the dorsalmost LVW region of devascularized animals ET-ir was significantly higher than in control and G-CSF samples ($p<0.001$).

In the ventral regions of the LVW Control, G-CSF and devascularized samples had similar average values: $0.81 \pm 0.29\ \mu m^2$, $1.08 \pm 0.14\ \mu m^2$ and $0.80 \pm 0.31\ \mu m^2$, respectively (Fig. 4B). No significant differences were found (Kruskal–Wallis). GFAP-ir associated to the dorsal and ventral LVW followed the same pattern (not shown).

### 2.6.2. *Subcallosal enlargement*

Simple observation of this region showed that cortical devascularization induced an important increase in area and intensity of ET-ir. However, morphological deformation hindered definition of equivalent ROIs in control and lesioned brains. Therefore, only G-CSF treated animals and their saline controls were submitted to quantitative evaluation.

The ROI for the SCE region was an irregular polygon including $ET^+$ structures comprised between the ependymal wall, the striatum and the CC. G-CSF-treated animals showed a 60% increase of total ET-ir compared with saline-treated controls

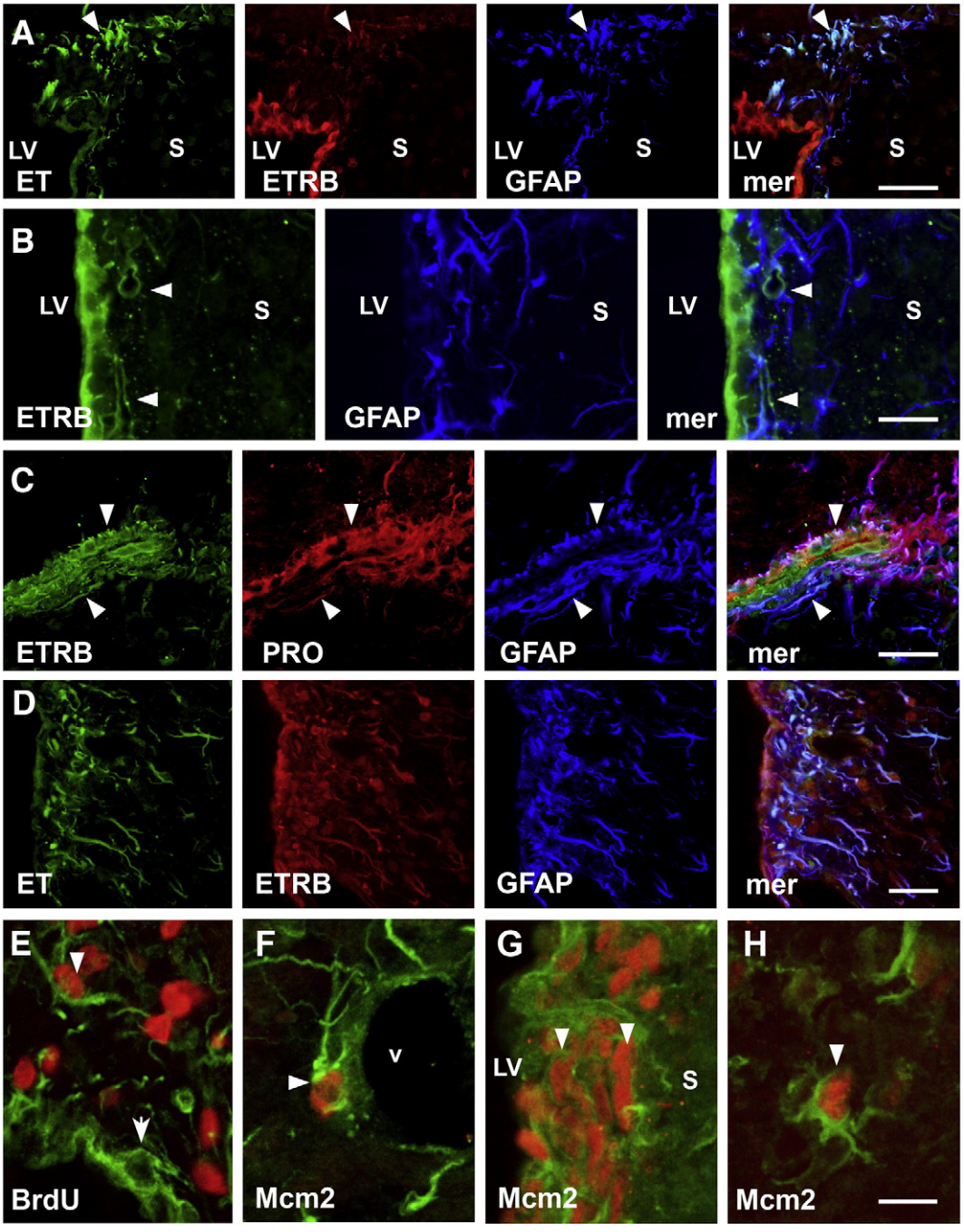

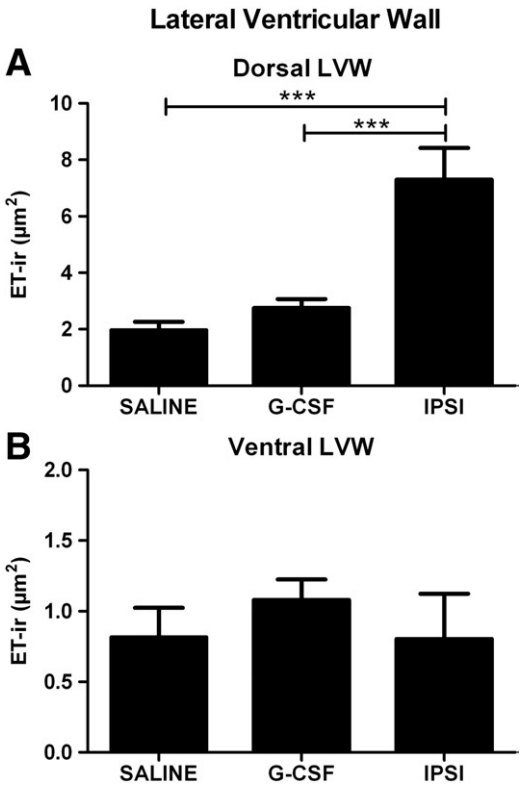


**Fig. 4 – Bars show the area occupied by ET-ir in two regions of the LVW: (A) the dorsalmost 80 μm, and (B) the following 100 μm. In control brains, the ET$^+$ area associated to the dorsal LVW almost duplicated that associated to the ventral region. G-CSF treatment slightly raised ET-ir associated to dorsal LVW, but a much larger increase appeared after ipsilateral devascularization (***$p<0.001$). The ventral LVW showed no significant changes.**

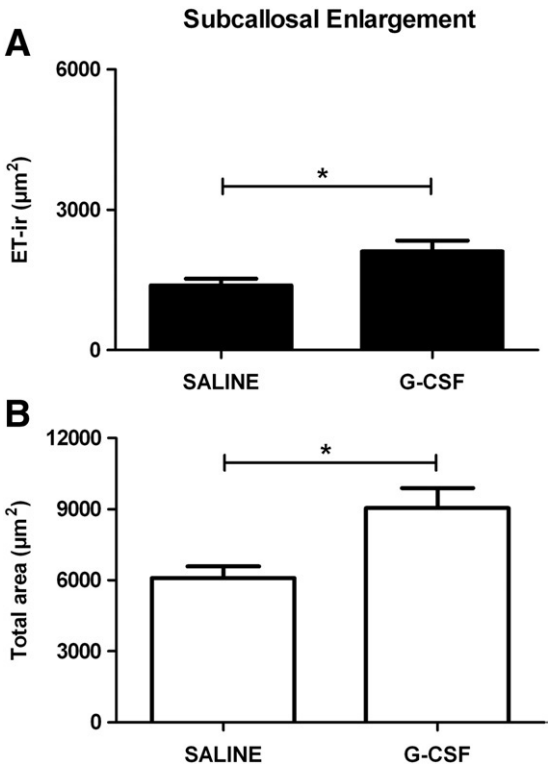


**Fig. 5 – (A) The ET-ir area enclosed within the SCE was 60% larger in G-CSF-treated animals than in saline-treated controls. (B) The total SCE area showed a similar increase (*$p<0.03$).**

(Fig. 5A), from 1832±183 μm$^2$ to 2994±362 μm$^2$. The difference was significant (*t* test, $p<0.003$). Total SCE area showed a parallel increase, pointing out that ET-ir density was similar in control and G-CSF-treated animals (Fig. 5B).

#### 2.6.3. *Dorsal ventricular wall*

To measure ET-ir associated to the DVW we defined a polygon of parallel borders following the shape of the luminal ependymal surface. The polygon had a constant width of 30 μm and included the EE and attached endothelinergic cells. To compare dorsal walls of different sizes, the area of associated ET-ir was divided over polygon length. Samples from 3 brains showed that G-CSF treatment decreased ET-ir in the DVW (Fig. 6A), from 4.2±0.3 μm$^2$ ($n=17$ sections) to 3.0±0.2 μm$^2$ ($n=20$ sections). Difference was significant, $p<0.011$ (*t* test).

#### 2.6.4. *Cingular bundle*

Since this callosal region has no clear lateral boundaries, we defined a fixed width (200 μm) rectangular ROI. The dorsal border was placed along the dorsalmost ET$^+$ cingular cells, whereas the ventral border was set at 40 μm from the ventricular luminal surface. Sections from control and G-CSF-treated animals showed the same cingular measures (heights: 336.0±10.61 μm vs. 330.4±14.90 μm; areas: 70690±2208 μm$^2$ vs. 69550±3155 μm$^2$). ET-ir was standardized to a 100 μm$^2$ area. G-CSF treatment increased cingular ET$^+$ structures, from 3.14±0.34 μm$^2$ ($n=22$) in control brains to 5.28±0.30 μm$^2$ ($n=23$) in G-CSF-treated brains (Fig. 6B). The difference was significant, $p<0.0001$ (*t* test).

## 3. Discussion

### 3.1. *Endothelin and neural stem cells*

Our findings show that ET and its receptor ETRB were selectively expressed in the SEZ and RMS, the adult neurogenic centers containing NSCs (Abrous et al., 2005). Ependymal cells also displayed ETRB-ir, but lacked ET-ir.

Distribution of ET$^+$ cells closely followed that of GFAP$^+$ subependymal astrocytes, which behave as NSCs (Alonso et al., 2008; Doetsch et al., 1999; Garcia et al., 2004; Platel et al., 2009; Seri et al., 2001). Endothelinergic cells also expressed PRO (or CD133), a stem cell marker used to isolate adult NSCs (Corti et al., 2007). ET, GFAP and PRO co-localized within apical cell processes traversing between ependymal cells, described as an essential feature of subependymal NSCs (Alvarez-Buylla et al., 1998; Danilov et al., 2009; Doetsch et al., 1999; Mirzadeh et al., 2008). However, we noted similar processes along the DVW, and probably also along the medial wall (Castañeda et al., in preparation). Consequently, trans-ependymal processes might be a property of astrocyte-like cells lying along every ventricular wall. They would not necessarily reflect stemness,

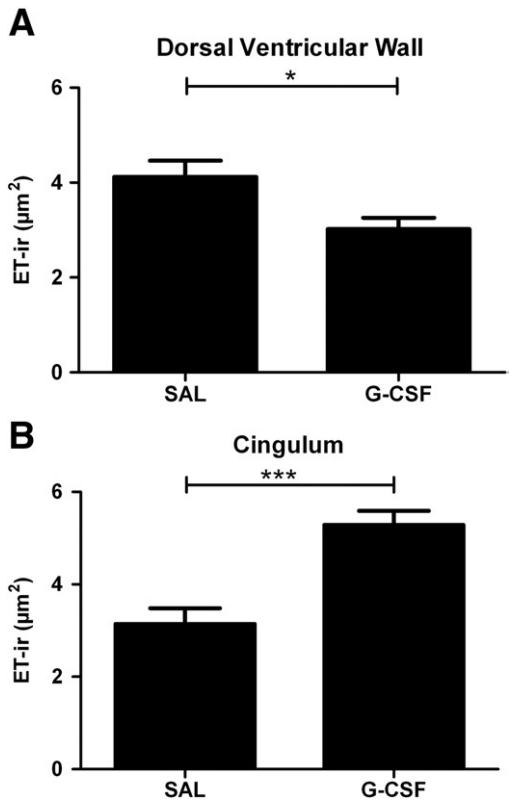


**Fig. 6 – (A) In the DVW, G-CSF induced a small but significant reduction ($p<0.02$) of associated ET-ir. (B) In the cingulum, the same treatment resulted in a large increase ($p<0.001$) of endothelinergic cells and processes ($^{***}p<0.001$).**

unless we assume that NSCs dwell around the whole adult ventricle, as recently suggested (Alvarez-Buylla et al., 2008).

The presence of PRO in subependymal astrocyte-like cells has not been detected by some authors (Coskun et al., 2008; Pfenninger et al., 2007). However, it is present in human RMS (Kam et al., 2009) and astrocytes of injured retina (Castañeda et al., in preparation). Discrepancies probably reflect differences in procedures. Since ependymal cells showed much stronger PRO-ir than subependymal cells, it would be easy to overlook cells with low PRO expression levels.

$ET^+$ cells labeled by BrdU or MCM2 cells represented a minor fraction of all subependymal proliferating nuclei, as expected from slow cyclers. Proliferative behavior of subependymal endothelinergic cells would resemble that of GFAP-expressing neural precursors (Doetsch et al., 1997; Garcia et al., 2004).

### 3.2. *Endothelin and the neurogenic niche*

Endothelin might also be present in other cells from the neurogenic niche. Besides NSCs, the subependymal region contains related cell phenotypes, such as transit amplifying progenitors, neuroblasts, astrocytes (B2 cells), and ependymal cells (Abrous et al., 2005; Doetsch et al., 1997). Most cells labeled by BrdU or Mcm2 lacked endothelinergic markers. Thus, the rapidly dividing transit amplifying progenitors and neuroblasts would not express endothelin.

On the other hand neuronal precursors and neuroblasts follow their characteristic "chain" migration within oriented glial tubes (Lois et al., 1996; Peretto et al., 1997). ET-ir could perhaps be associated to subependymal astrocytes forming those glial tubes. This is a likely possibility, since all endothelinergic cells also expressed the astrocytic marker GFAP.

Subependymal and RMS endothelinergic cells would not represent reactive glial cells. The latter appear around the devascularized region and have thicker and coarser processes than subependymal cells (Castañeda et al., in preparation).

Endothelinergic blockers have neuroprotective effects after experimental brain infarct (Barone et al., 1995; Stenman et al., 2007) and traumatic brain injury (Kreipke et al., 2009). These are immediate effects that have been associated to the regulation of vascular perfusion in the injured brain (Leung et al., 2009). Their relationship to the subependymal neurogenic niche remains to be established.

### 3.3. *Endothelinergic cells in the cingulum*

Co-localization of ET-ir with PRO- and GFAP-ir suggests that cingular endothelinergic cells might belong to the SEZ gliogenic or radial migration pathway (Suzuki and Goldman, 2003). This lineage arises from subependymal astrocyte-like cells (Colak et al., 2008; Menn et al., 2006) and originates neocortical astrocytes and oligodendrocytes (Zerlin et al., 2004). PRO transcripts have been detected in developing oligodendrocytes and astrocytes (Corbeil et al., 2009). Our findings further suggest that callosal endothelinergic cells could be related to those in the DVW. Thus, G-CSF decreased ET-ir associated to the DVW, but increased cingular ET-ir. The radial migration pathway would also be activated by cortical injury, as suggested by the appearance of BrdU and Mcm2 labeling in cingular $ET^+$ cells in lesioned brains.

### 3.4. *A possible role of ETRB and PRO in the ependymal epithelium*

Ependymal cells showed strong ETRB-ir all around the ventricular lumen. By contrast, only the lateral and dorsal walls displayed strong PRO-ir. Ependymal cells together with subependymal astrocytes might serve as adult NSCs (Coskun et al., 2008; Johansson et al., 1999; Zhang et al., 2007). Ependymal PRO-ir only appeared in the ventricular walls in contact with subependymal endothelinergic cells, presumably representing NSCs. Exposure of ependymal cells to endothelin, or other molecules, derived from subependymal cells might perhaps modulate PRO expression and their stemness.

## 4. Conclusions

Although further studies are required to understand the role of endothelins and their receptors on adult neurogenesis, it is tempting to speculate that autocrine and paracrine endothelinergic stimulation could perhaps regulate proliferation and differentiation of adult murine neural precursor cells. Endothelin stimulates [$^3$H]-thymidine incorporation (Morishita et al., 2007; Shinohara et al., 2004) and inhibits migration

of embryonic neural progenitor cells (Mizuno et al., 2005). Neurospheres from embryonic or adult spinal cord express ETRB, and incubation with ET-1 or ET-3 stimulates their growth (Deleyrolle et al., 2006). In addition, available evidence supports a role of the endothelinergic system in brain cancer growth (Paolillo et al., 2006).

It has been proposed that a neural stem cell niche should preserve stem cells in a multipotent, and mitotically, and metabolically quiescent state (Coskun et al., 2008). The different distribution of endothelinergic molecules in ependymal cells and subependymal astrocytes could originate interactions allowing persistence of multipotentiality or acquisition of differentiated features. In ependymal cells, the presence of ETRB without ET expression might result in conservation of multipotentiality. In subependymal cells, autocrine endothelinergic signaling could perhaps promote proliferation and differentiation of neural and glial precursors.

## 5. Experimental procedures

### 5.1. *Animals*

Male C57Bl/6 mice (6–8 weeks old) were bred and cared according to the "U.S. Public Health Service's Policy on Humane Care Research Use of Laboratory Animals (PHS policy)".

### 5.2. *Immunohistochemistry and immunofluorescence*

Mice were deeply anesthetized (chloral hydrate, 800 mg/kg) and perfused through the heart with 4% paraformaldehyde solution in 0.1 M phosphate buffer, pH 7.3. The brains were cryopreserved in graded sucrose solutions and sucrose–OCT compound mixes. 3 mm slices were obtained using an acrylic matrix for coronal sections (David Kopf Instruments, Tujunga, Ca). Specimens were frozen in $N_2$-cooled acetone. Cryosections (14 μm) were stained with Neutral Red or processed for immunohistochemistry. Primary antibodies are described in Table 1.

BrdU detection required DNA denaturalization in 2 N HCl plus 5% Triton-X100 (Sigma-Aldrich Co, St Louis MO) during 60 min at room temperature. After rapid washing with 0.1 M phosphate buffer and PBS, sections were processed for immunohistochemistry or immunofluorescence.

Biotinylated secondary antibodies followed by avidin-biotinylated peroxidase complex (Vectastain® Elite ABC-peroxidase kit, Vector Labs, Burlingame, CA) were used for immunoenzymatic detection. A color reaction was obtained using nickel-enhanced diaminobencidine staining (Suburo et al., 1992).

Fluorescein isothiocyanate-, lissamine rhodamine- or Cy5-conjugated anti-rabbit, antimouse or anti-guinea pig IgGs (Jackson Immunoresearch Laboratories, West Grove, PA), Alexa 546 anti-chicken A11040, Alexa 546 anti-goat A11056, Alexa 633 anti-rabbit A21071 and Alexa 647 anti-rat A21472 (Invitrogen Co. Carlsbad, CA) were used for immunofluorescence. Confocal images were obtained with a Laser Scanning System Radiance 2000 (BioRad, Hemel Hempstead, UK). The 488 line of the argon laser, the 543 line of a helium-neon laser, and a 633 nm line from a diode laser were sequentially used. Cytoplasmic co-localization was evaluated in 1 μm thick optical sections. Optic projections and merged images were produced with Confocal Assistant Software (BioRad, Hemel Hempstead, UK).

Controls, omitting incubation with primary antibodies, were made for every immunostaining procedure. Tissue blocks always included slices from non-treated and treated animals. Only simultaneously processed samples were used for comparisons.

### 5.3. *BrdU incorporation*

Mice received 2 BrdU injections (150 mg/kg each, ip), 24 and 1 h before fixation. Double immunofluorescence labeling was done as described above.

### 5.4. *Cortical devascularization and G-CSF treatment*

The right cerebral hemisphere was submitted to small cortical lesions using a modification of the devascularization procedure described for rats (Bartnik et al., 2001). Anesthesia was induced with chloral hydrate (400 mg/kg, ip.), and lidocaine gel (Astra-Zeneca, Argentina) applied to the outer ears. Mice were placed in a stereotaxic frame, the cranium was exposed and a rectangular piece of bone was drilled over the right hemisphere (+3 to −2 mm anterioposterior, and 0.5 to 2.5 mm lateral to bregma). The pial membrane overlying cortical area M1 and neighboring regions of areas M2 and S1 was gently lifted with a blunt hook. Animals were euthanatized after 5 days, since this time period allows a significant increase in SEZ cell number (Gotts and Chesselet, 2005) and partial recovery of motor deficit (Castañeda et al., in preparation).

Two groups ($n=6$ each) of non-operated mice were injected with saline or G-CSF (Neutromax, Biosidus, 50 mg/kg/day) for 5 days. This time is enough to detect significant improvement of motor behavior in mice with cortical devascularization (Castañeda et al., in preparation).

### 5.5. *Image analysis*

Coronal brain slices between +1 and bregma (A–P) were serially sectioned. Each 10th section was immunostained with ET or GFAP antibodies and photographed at 40×. A blinded operator evaluated montages of both hemispheres. ROIs for lateral and dorsal ventricular walls, the SCE enlargement and callosal cingulum are described in the text. Adobe Photoshop CS4 Extended was used to select the ROIs. After measuring total ROI area, height and length, immunoreactive area ($\mu m^2$) was thresholded and quantified using automatic adjustment and measurement sequences. Background intensities were determined from the histogram of pixel values for pixels within the ROIs. The same background values were applied to all measured images.

### 5.6. *Statistical analysis*

GraphPad Prism version 4.00 for Windows (GraphPad Software, San Diego California USA) was used for statistical analysis. Results are expressed as mean + standard error unless otherwise stated.

## Acknowledgments

MMC and MAC are research fellows from the Consejo Nacional de Investigaciones Científicas y Técnicas (CONICET) and ANPCyT, MINCYT, Argentina, respectively. MML-V was a training fellow from the Comisión de Investigaciones Científicas de la Provincia de Buenos Aires (CIC), and AMS is Principal Researcher from CONICET. Studies reported here were funded by grants from Universidad Austral, 2006 and 2007, and ANPCyT (21399/2004). We are very grateful to Guillermo Gastón and Soledad Arregui for their skilful technical assistance.

## REFERENCES

Abrous, D.N., Koehl, M., Le Moal, M., 2005. Adult neurogenesis: from precursors to network and physiology. Physiol. Rev. 85, 523–569.

Alonso, M., Ortega-Perez, I., Grubb, M.S., Bourgeois, J.P., Charneau, P., Lledo, P.M., 2008. Turning astrocytes from the rostral migratory stream into neurons: a role for the olfactory sensory organ. J. Neurosci. 28, 11089–11102.

Alvarez-Buylla, A., Garcia-Verdugo, J.M., Mateo, A.S., Merchant-Larios, H., 1998. Primary neural precursors and intermitotic nuclear migration in the ventricular zone of adult canaries. J. Neurosci. 18, 1020–1037.

Alvarez-Buylla, A., Kohwi, M., Nguyen, T.M., Merkle, F.T., 2008. The heterogeneity of adult neural stem cells and the emerging complexity of their niche. Cold Spring Harb. Symp. Quant. Biol. 73, 357–365.

Bartnik, B.L., Kendall, E.J., Obenaus, A., 2001. Cortical devascularization: quantitative diffusion weighted magnetic resonance imaging and histological findings. Brain Res. 915, 133–142.

Barone, F.C., White, R.F., Elliott, J.D., Feuerstein, G.Z., Ohlstein, E.H., 1995. The endothelin receptor antagonist SB 217242 reduces cerebral focal ischemic brain injury. J. Cardiovasc. Pharmacol. 26 (Suppl 3), S404–S407.

Colak, D., Mori, T., Brill, M.S., Pfeifer, A., Falk, S., Deng, C., Monteiro, R., Mummery, C., Sommer, L., Gotz, M., 2008. Adult neurogenesis requires Smad4-mediated bone morphogenic protein signaling in stem cells. J. Neurosci. 28, 434–446.

Corbeil, D., Joester, A., Fargeas, C.A., Jaszai, J., Garwood, J., Hellwig, A., Werner, H.B., Huttner, W.B., 2009. Expression of distinct splice variants of the stem cell marker prominin-1 (CD133) in glial cells. Glia 57, 860–874.

Corti, S., Nizzardo, M., Nardini, M., Donadoni, C., Locatelli, F., Papadimitriou, D., Salani, S., Del Bo, R., Ghezzi, S., Strazzer, S., Bresolin, N., Comi, G.P., 2007. Isolation and characterization of murine neural stem/progenitor cells based on Prominin-1 expression. Exp. Neurol. 205, 547–562.

Coskun, V., Wu, H., Blanchi, B., Tsao, S., Kim, K., Zhao, J., Biancotti, J.C., Hutnick, L., Krueger Jr., R.C., Fan, G., de Vellis, J., Sun, Y.E., 2008. CD133$^{+}$ neural stem cells in the ependyma of mammalian postnatal forebrain. Proc. Natl. Acad. Sci. U. S. A. 105, 1026–1031.

Danilov, A.I., Gomes-Leal, W., Ahlenius, H., Kokaia, Z., Carlemalm, E., Lindvall, O., 2009. Ultrastructural and antigenic properties of neural stem cells and their progeny in adult rat subventricular zone. Glia 57, 136–152.

Davenport, A.P., Maguire, J.J., 2006. Endothelin. Handb. Exp. Pharmacol. 295–329.

Deleyrolle, L., Marchal-Victorion, S., Dromard, C., Fritz, V., Saunier, M., Sabourin, J.C., Tran Van Ba, C., Privat, A., Hugnot, J.P., 2006. Exogenous and fibroblast growth factor 2/epidermal growth factor-regulated endogenous cytokines regulate neural precursor cell growth and differentiation. Stem Cells 24, 748–762.

Diederich, K., Sevimli, S., Dorr, H., Kosters, E., Hoppen, M., Lewejohann, L., Klocke, R., Minnerup, J., Knecht, S., Nikol, S., Sachser, N., Schneider, A., Gorji, A., Sommer, C., Schabitz, W.R., 2009. The role of granulocyte-colony stimulating factor (G-CSF) in the healthy brain: a characterization of G-CSF-deficient mice. J. Neurosci. 29, 11572–11581.

Doetsch, F., Garcia-Verdugo, J.M., Alvarez-Buylla, A., 1997. Cellular composition and three-dimensional organization of the subventricular germinal zone in the adult mammalian brain. J. Neurosci. 17, 5046–5061.

Doetsch, F., Caille, I., Lim, D.A., Garcia-Verdugo, J.M., Alvarez-Buylla, A., 1999. Subventricular zone astrocytes are neural stem cells in the adult mammalian brain. Cell 97, 703–716.

Duan, X., Kang, E., Liu, C.Y., Ming, G.L., Song, H., 2008. Development of neural stem cell in the adult brain. Curr. Opin. Neurobiol. 18, 108–115.

Dubreuil, V., Marzesco, A.M., Corbeil, D., Huttner, W.B., Wilsch-Brauninger, M., 2007. Midbody and primary cilium of neural progenitors release extracellular membrane particles enriched in the stem cell marker prominin-1. J. Cell Biol. 176, 483–495.

Ehrenreich, H., Anderson, R.W., Ogino, Y., Rieckmann, P., Costa, T., Wood, G.P., Coligan, J.E., Kehrl, J.H., Fauci, A.S., 1991. Selective autoregulation of endothelins in primary astrocyte cultures: endothelin receptor-mediated potentiation of endothelin-1 secretion. New Biol. 3, 135–141.

Gadea, A., Schinelli, S., Gallo, V., 2008. Endothelin-1 regulates astrocyte proliferation and reactive gliosis via a JNK/c-Jun signaling pathway. J. Neurosci. 28, 2394–2408.

Garcia, A.D., Doan, N.B., Imura, T., Bush, T.G., Sofroniew, M.V., 2004. GFAP-expressing progenitors are the principal source of constitutive neurogenesis in adult mouse forebrain. Nat. Neurosci. 7, 1233–1241.

Gotts, J.E., Chesselet, M.F., 2005. Migration and fate of newly born cells after focal cortical ischemia in adult rats. J. Neurosci. Res. 80, 160–171.

Gritti, A., Bonfanti, L., Doetsch, F., Caille, I., Alvarez-Buylla, A., Lim, D.A., Galli, R., Verdugo, J.M., Herrera, D.G., Vescovi, A.L., 2002. Multipotent neural stem cells reside into the rostral extension and olfactory bulb of adult rodents. J. Neurosci. 22, 437–445.

Iribarne, M., Ogawa, L., Torbidoni, V., Dodds, C.M., Dodds, R.A., Suburo, A.M., 2008. Blockade of endothelinergic receptors prevents development of proliferative vitreoretinopathy in mice. Am. J. Pathol. 172, 1030–1042.

Ishikawa, N., Takemura, M., Koyama, Y., Shigenaga, Y., Okada, T., Baba, A., 1997. Endothelins promote the activation of astrocytes in rat neostriatum through ET(B) receptors. Eur. J. Neurosci. 9, 895–901.

Johansson, C.B., Momma, S., Clarke, D.L., Risling, M., Lendahl, U., Frisen, J., 1999. Identification of a neural stem cell in the adult mammalian central nervous system. Cell 96, 25–34.

Kam, M., Curtis, M.A., McGlashan, S.R., Connor, B., Nannmark, U., Faull, R.L., 2009. The cellular composition and morphological organization of the rostral migratory stream in the adult human brain. J. Chem. Neuroanat. 37, 196–205.

Koyama, Y., Tsujikawa, K., Matsuda, T., Baba, A., 2003. Intracerebroventricular administration of an endothelin ETB receptor agonist increases expressions of GDNF and BDNF in rat brain. Eur. J. Neurosci. 18, 887–894.

Koyama, Y., Tsujikawa, K., Matsuda, T., Baba, A., 2005. Endothelin increases expression of exon III- and exon IV-containing brain-derived neurotrophic factor transcripts in cultured astrocytes and rat brain. J. Neurosci. Res. 80, 809–816.

Kreipke, C.W., Schafer, P.C., Rossi, N.F., Rafols, J.A., 2009. Differential effects of endothelin receptor A and B antagonism on cerebral hypoperfusion following traumatic brain injury. Neurol. Res. ([Epub ahead of print] PMID: 19570328).

Leung, J.W., Chung, S.S., Chung, S.K., 2009. Endothelial endothelin-1 over-expression using receptor tyrosine kinase tie-1 promoter leads to more severe vascular permeability and blood brain barrier breakdown after transient middle cerebral artery occlusion. Brain Res. 1266, 121–129.

Lois, C., Garcia-Verdugo, J.M., Alvarez-Buylla, A., 1996. Chain migration of neuronal precursors. Science 271, 978–981.

Maslov, A.Y., Barone, T.A., Plunkett, R.J., Pruitt, S.C., 2004. Neural stem cell detection, characterization, and age-related changes in the subventricular zone of mice. J. Neurosci. 24, 1726–1733.

Menn, B., Garcia-Verdugo, J.M., Yaschine, C., Gonzalez-Perez, O., Rowitch, D., Alvarez-Buylla, A., 2006. Origin of oligodendrocytes in the subventricular zone of the adult brain. J. Neurosci. 26, 7907–7918.

Mirzadeh, Z., Merkle, F.T., Soriano-Navarro, M., Garcia-Verdugo, J.M., Alvarez-Buylla, A., 2008. Neural stem cells confer unique pinwheel architecture to the ventricular surface in neurogenic regions of the adult brain. Cell Stem Cell 3, 265–278.

Mizuno, N., Kokubu, H., Sato, M., Nishimura, A., Yamauchi, J., Kurose, H., Itoh, H., 2005. G protein-coupled receptor signaling through Gq and JNK negatively regulates neural progenitor cell migration. Proc. Natl. Acad. Sci. U. S. A. 102, 12365–12370.

Morishita, R., Ueda, H., Ito, H., Takasaki, J., Nagata, K., Asano, T., 2007. Involvement of Gq/11 in both integrin signal-dependent and -independent pathways regulating endothelin-induced neural progenitor proliferation. Neurosci. Res. 59, 205–214.

Naidoo, V., Naidoo, S., Mahabeer, R., Raidoo, D.M., 2005. Localization of the endothelin system in human diffuse astrocytomas. Cancer 104, 1049–1057.

Ostrow, L.W., Sachs, F., 2005. Mechanosensation and endothelin in astrocytes—hypothetical roles in CNS pathophysiology. Brain Res. Brain Res. Rev. 48, 488–508.

Paolillo, M., Barbieri, A., Zanassi, P., Schinelli, S., 2006. Expression of endothelins and their receptors in glioblastoma cell lines. J. Neurooncol. 79, 1–7.

Paxinos, G., Franklin, K.B.J., 2001. The Mouse Brain in Stereotaxic Coordinates. Academic Press, San Diego.

Peretto, P., Merighi, A., Fasolo, A., Bonfanti, L., 1997. Glial tubes in the rostral migratory stream of the adult rat. Brain Res. Bull. 42, 9–21.

Pfenninger, C.V., Roschupkina, T., Hertwig, F., Kottwitz, D., Englund, E., Bengzon, J., Jacobsen, S.E., Nuber, U.A., 2007. CD133 is not present on neurogenic astrocytes in the adult subventricular zone, but on embryonic neural stem cells, ependymal cells, and glioblastoma cells. Cancer Res. 67, 5727–5736.

Platel, J.C., Gordon, V., Heintz, T., Bordey, A., 2009. GFAP-GFP neural progenitors are antigenically homogeneous and anchored in their enclosed mosaic niche. Glia 57, 66–78.

Riechers, C.C., Knabe, W., Siren, A.L., Gariepy, C.E., Yanagisawa, M., Ehrenreich, H., 2004. Endothelin B receptor deficient transgenic rescue rats: a rescue phenomenon in the brain. Neuroscience 124, 719–723.

Rogers, S.D., Peters, C.M., Pomonis, J.D., Hagiwara, H., Ghilardi, J.R., Mantyh, P.W., 2003. Endothelin B receptors are expressed by astrocytes and regulate astrocyte hypertrophy in the normal and injured CNS. Glia 41, 180–190.

Seri, B., Garcia-Verdugo, J.M., McEwen, B.S., Alvarez-Buylla, A., 2001. Astrocytes give rise to new neurons in the adult mammalian hippocampus. J. Neurosci. 21, 7153–7160.

Shinohara, H., Udagawa, J., Morishita, R., Ueda, H., Otani, H., Semba, R., Kato, K., Asano, T., 2004. Gi2 signaling enhances proliferation of neural progenitor cells in the developing brain. J. Biol. Chem. 279, 41141–41148.

Stenman, E., Jamali, R., Henriksson, M., Maddahi, A., Edvinsson, L., 2007. Cooperative effect of angiotensin AT(1) and endothelin ET(A) receptor antagonism limits the brain damage after ischemic stroke in rat. Eur. J. Pharmacol. 570, 142–148.

Suburo, A.M., Wheatley, S.C., Horn, D.A., Gibson, S.J., Jahn, R., Fischer-Colbrie, R., Wood, J.N., Latchman, D.S., Polak, J.M., 1992. Intracellular redistribution of neuropeptides and secretory proteins during differentiation of neuronal cell lines Neuroscience 46, 881–889.

Suzuki, S.O., Goldman, J.E., 2003. Multiple cell populations in the early postnatal subventricular zone take distinct migratory pathways: a dynamic study of glial and neuronal progenitor migration. J. Neurosci. 23, 4240–4250.

Tabernero, A., Sanchez-Alvarez, R., Medina, J.M., 2006. Increased levels of cyclins D1 and D3 after inhibition of gap junctional communication in astrocytes. J. Neurochem. 96, 973–982.

Torbidoni, V., Iribarne, M., Ogawa, L., Prasanna, G., Suburo, A.M., 2005. Endothelin-1 and endothelin receptors in light-induced retinal degeneration. Exp. Eye Res. 81, 265–275.

Zerlin, M., Milosevic, A., Goldman, J.E., 2004. Glial progenitors of the neonatal subventricular zone differentiate asynchronously, leading to spatial dispersion of glial clones and to the persistence of immature glia in the adult mammalian CNS. Dev. Biol. 270, 200–213.

Zhang, R.L., Zhang, Z.G., Wang, Y., LeTourneau, Y., Liu, X.S., Zhang, X., Gregg, S.R., Wang, L., Chopp, M., 2007. Stroke induces ependymal cell transformation into radial glia in the subventricular zone of the adult rodent brain. J. Cereb. Blood Flow Metab. 27, 1201–1212.

Zhang, R.L., Zhang, Z.G., Chopp, M., 2008. Ischemic stroke and neurogenesis in the subventricular zone. Neuropharmacology 55, 345–352.